Study of a passive pitching rotor using blade element momentum theory coupled to a rigid-body model

Krishnan, Navaneetha; Viré, Axelle; Klippe, Rikus Van De

DOI
10.1088/1742-6596/2265/3/032057

Publication date
2022

Document Version
Final published version

Published in
Journal of Physics: Conference Series

Study of a passive pitching rotor using blade element momentum theory coupled to a rigid-body model

Study of a passive pitching rotor using blade element momentum theory coupled to a rigid-body model

Navaneetha Krishnan[1], Axelle Viré[1], and Rikus van de Klippe[2]

[1] Dept. of Wind Energy, Faculty of Aerospace Engineering, Delft University of Technology, Kluyverweg 1, 2629HS, Delft, the Netherlands.
[2] TouchWind B.V., High Tech Campus 29, 5656AE, Eindhoven, the Netherlands

E-mail: a.c.vire@tudelft.nl

Abstract. Misaligned wind turbine rotors experience uneven loads because of two effects: dissymmetry of lift, and skewed wake effect. Rotor-crafts that have a similar problem introduce various mechanisms to combat this — one of them is to add a δ_3-hinge. The hinge provides the blade with an additional degree of freedom to relieve the unbalanced loads; in theory, it is a self-correcting mechanism. In this work, we couple a blade element momentum (BEM) approach for the aerodynamics to a rigid-body model that simulates the hinge rotation. The results from BEM are used to identify the working mechanisms of the hinged rotor and highlight the strengths and weaknesses of such a rotor.

1. Introduction

Offshore wind energy will play a key role in the global energy transition. In this context, floating offshore wind turbines (FOWTs) are believed to be a key enabler to massively increase the installed capacity of offshore wind power, as these turbines can be installed in seas much deeper than with existing bottom-fixed turbines. The main FOWTs currently being developed use conventional three-bladed wind turbine rotors. However, because the loads and dynamics of FOWTs are different than for bottom-fixed turbines, innovative wind turbine rotors could be more attractive for floating applications. The company TouchWind B.V. has proposed a two-bladed passive pitch rotor that uses a hinge mechanism, so that the lift force of the rotor can regulate the orientation of the rotor blade relative to the wind flow. The purpose of this work is to investigate in more detail the working principles of this rotor using a blade element momentum (BEM) aerodynamic model coupled to a rigid-body dynamics model of the hinge.

A wind turbine yawed at an angle γ, or tilted at an angle θ, is misaligned with the wind, and experiences load variations on the blade due to dissymmetry of lift and skewed wake effect. Assuming wind is from the left and the blade is rotating counter-clockwise, fig. 1 plots the normalised integral lift experienced by a blade under different conditions: (a) the ideal case with uniform loading round the clock, (b) with dissymmetry of lift, the approaching side (red) generates a higher lift than the retreating side (black), (c) with skewed wake effect, the upwind side (red) is loaded heavier than the downwind side (black), and (d) the net lift experienced by a misaligned blade. The imbalance in the aerodynamic loads experienced by the blades during the rotation results in an undesirable aerodynamic moment acting on the rotor. In a two-bladed configuration, a blade in the red region experiences a higher aerodynamic load than the other

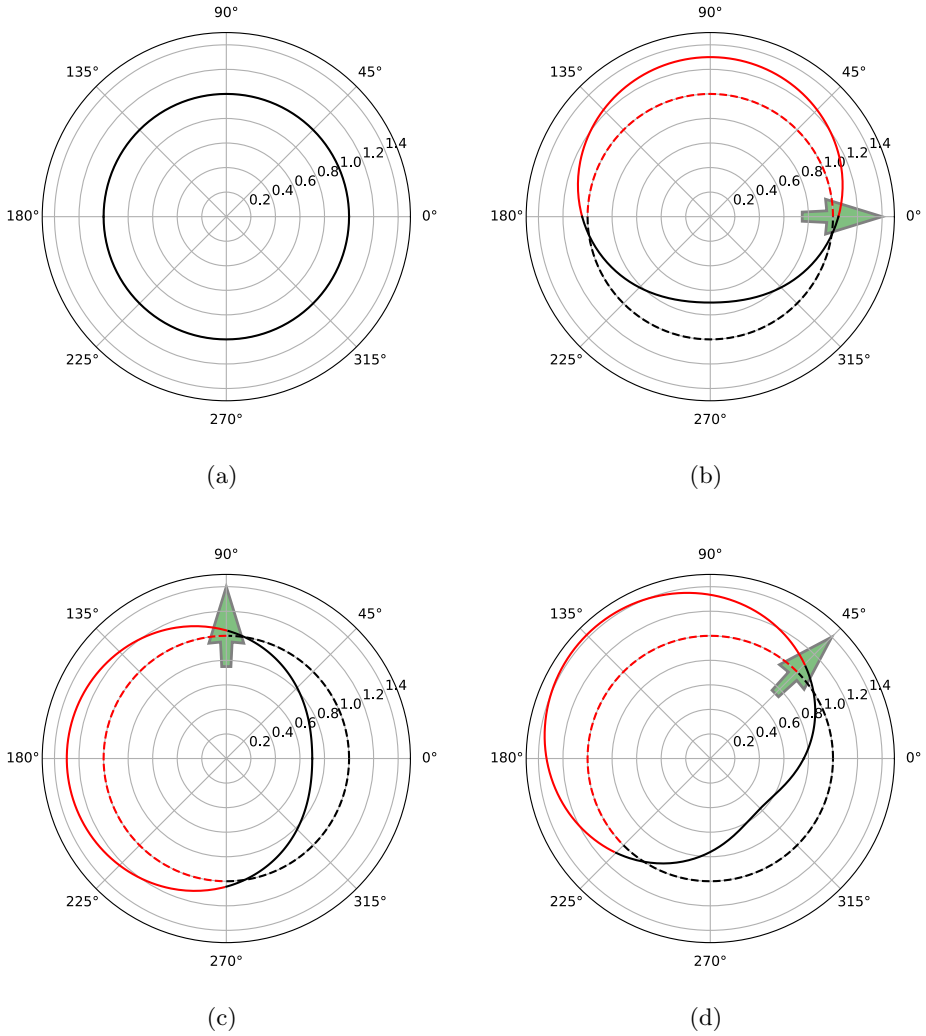

Figure 1: Normalised lift integral experienced by a blade during a rotation. Wind is from the left and the rotor is in anti-clockwise rotation. Green arrows point in the direction of the maxima of the external torque. (a) In the ideal case, the blade would see uniform loading throughout the rotation. (b) Dissymmetry of lift divides the rotation into an approaching half (red) and a retreating half (black). (c) Skewed wake effect divides the rotation into an upwind side (red) and a downwind side (black). (d) Net lift experience by the blade in a misaligned rotor.

blade in the black region. Thus, the maxima of the net aerodynamic moment on the rotor are as shown by green arrows in fig. 1. Torque arising from the dissymmetry of lift is maximum when the blades are orthogonal to the wind, whilst torque from the skewed wake effect is maximum when the blades are aligned with the wind. Combined, the torque on the blade is maximum when the rotor is in the approaching-upwind quadrant, with the direction of the torque pointing 90° behind in the approaching-downwind quadrant. In this paper, we look at a δ_3 coupling used in rotor-crafts to tackle the same problem [1].

The δ_3 coupling, as the name implies, adds a hinge at an angle $90° - \delta_3$ with respect to the blade axis. This introduces a pitch-teeter degree of freedom to the rotor. In fig. 2(a)

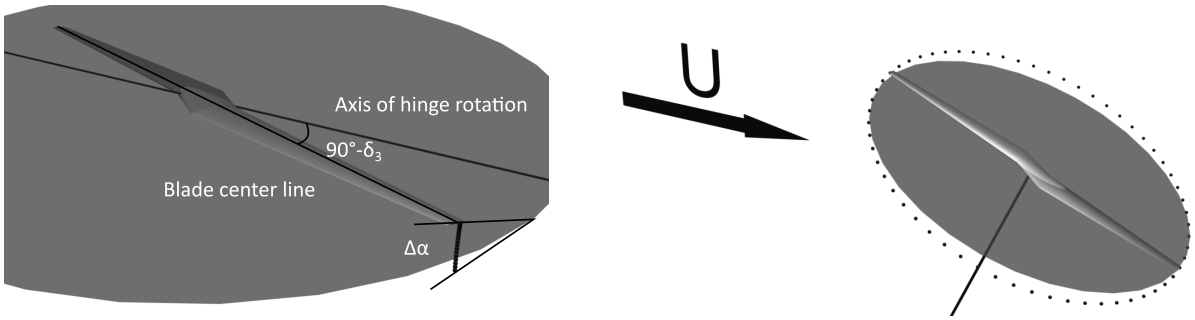

(a) (b)

Figure 2: (a) With the δ_3 hinge, the rotor has the freedom to rotate up/down about the hinge axis, and adjust its pitch in the process. (b) A misaligned hinged rotor in wind can rotate away from the grey reference rotor plane to a path of even loading.

the pitch decreases when the blade tilts up from the grey reference rotor plane. The pitch-teeter ratio (η_y/η_z) depends on the δ_3 angle as, $-\tan(\delta_3 + \varphi_i)$; φ_i is the blade offset angle. A negative value for the pitch-teeter ratio leads to an inverse coupling between pitch and teeter, and adds 'restoring' aerodynamic forces to a rotor experiencing unbalanced aerodynamic moments. The rotor can rotate away from the fixed plane, and find a trajectory (dotted path in fig. 2(b)) in which load variations are reduced. Studies with simplified equations for the teetering motion have arrived at the same conclusion; a positive δ_3 added stability and a negative δ_3 was destabilising [2,3]. A series of works on two-bladed rotors looked at mainly the furling control of teetered rotors, and suggested that a positive δ_3 coupling added stability below the stall region of the blade [4–8]. A later study derived a more accurate set of equations for the teetering motion and looked at how the rotor responds to varying aerodynamic moments [9]. Another point worth noticing is that, only a 2-bladed configuration is stable on a single hinge rotor. For rotors with more than 2 blades, depending on the blade offset, some of the blades will experience a positive pitch-teeter coupling.

With the degree of freedom offered by the hinge, the external torque on the rotor induces gyroscopic precession. Neglecting the rotation about the hinge, the major component of angular momentum on the rotor is the one from the rotation of the rotor, and points out of the paper in fig. 1 (normal of the reference plane in fig. 2). Gyroscopic precession will try to tilt the angular momentum vector in the direction of the external torque, i.e., the rotor will start tilting in the direction of the external torque (dotted path in fig. 2(b)).

2. Methodology

2.1. Blade Element Momentum theory

In this work, the classical BEM theory is modified to account for the rotation of the hinge. With the angular velocity of the rotor defined as Ω, and the rate of hinge rotation defined as $\dot{\eta}$, the linear velocity of a 2D aerofoil section at a radius of r is,

$$\mathbf{V} = r(\Omega \sin(\delta_3 + \varphi_i)\sin(\eta) + \dot{\eta}\cos(\delta_3 + \varphi_i))\hat{\mathbf{b}}_{in} - r\Omega\cos(\eta)\hat{\mathbf{b}}_{it}. \quad (1)$$

$\mathbf{b}_i$ are the unit vectors of the i^{th} blade reference frame. Because of the hinge rotation, along with the tangential component (t), the rotor has a normal component (n) of velocity. From here, the standard BEM procedure is used to compute the integral aerodynamic moment on the entire rotor ($\mathbf{M}$). In this paper, we use a convergence guaranteed algorithm [10], that provides a residual function with defined regions to search for the solution.

Table 1: Parameters of the test rotor.

Rotor diameter	1.2 m	δ_3	$arctan(2) \approx 63.43°$
Hub diameter	0.06 m	Inertia	$\begin{bmatrix} 0.5 & 0 & 0 \\ 0 & 0.5 & -0.02 \\ 0 & -0.02 & 0.01 \end{bmatrix}^B$ $kg \cdot m^2$
Root chord	0.1 m		
Tip chord	0.01 m		

2.2. Rigid body dynamics
Using Kane's method [11], we derive the acceleration of the hinge rotation, $\ddot{\eta}$, of the rotor considered as rigid as,

$$\ddot{\eta} = (\Omega^2 \sigma_0 + M_y \cos(\delta_3) - M_z \sin(\delta_3))/\sigma_1, \tag{2a}$$

$$\sigma_0 = \begin{aligned} &- I_{xx} \sin(2\eta)/2 + I_{xy}(1 - 2\sin^2(\eta)) \sin(\delta_3) + I_{yy} \sin^2(\delta_3) \sin(\eta) \cos(\eta) + \\ &I_{yz}(\cos(2(\delta_3 - \eta)) - \cos(2(\delta_3 + \eta)))/4 + I_{zx}(1 - 2\sin^2(\eta)) \cos(\delta_3) + I_{zz} \sin(\eta) \cos^2(\delta_3) \cos(\eta) \end{aligned} \tag{2b}$$

$$\sigma_1 = I_{yy} \cos^2(\delta_3) - I_{yz} \sin(2\delta_3) + I_{zz} \sin^2(\delta_3), \tag{2c}$$

where $\bar{\bar{\mathbf{I}}}$ is the symmetric mass moment of inertia tensor of the rotor. We can use $\ddot{\eta}$ in a system of ODEs to find $\dot{\eta}$, i.e.,

$$\begin{bmatrix} \psi & \Omega & \eta & \dot{\eta} \end{bmatrix}' = \begin{bmatrix} \Omega & 0 & \dot{\eta} & \ddot{\eta} \end{bmatrix}. \tag{3}$$

In the solution presented above for $\ddot{\eta}$, angular acceleration is assumed to be zero, and therefore, we set $\Omega' = 0$ in the ODE system. Non-zero angular acceleration of the rotor would simply generate a more complex solution for $\ddot{\eta}$, but is not in the scope of this paper. We integrate this initial value problem using a 4^{th} order Runge-Kutta algorithm.

The rigid body solver and the BEM solver are coupled using an explicit time stepping scheme, where the two models step in time in a staggered manner. However, within the ODE solver, a linear interpolation is used to obtain aerodynamic moments ($\mathbf{M}$) in the Runge-Kutta sub-time-step levels.

3. Results

Details of the rotor used in this paper are given in table 1. Chord varies linearly over span and the blade has no twist. Based on our definitions, I_{xx} (rotation) and I_{yy} (teeter) are the dominant components of inertia, and I_{zz} is the inertia about the pitching axis. With these parameters, we derive three rotors by changing the blade aerofoil used: F_1 and F_2, two idealised aerofoils, and F_3, a NACA4412 aerofoil. The idealised aerofoils have no stall or drag, and have a lift coefficient $C_L = 2\pi\alpha$ and $C_L = \pi\alpha$, for F_1 and F_2, respectively. We use the idealised aerofoil to remove the effects of stall from our analysis. For F_3, we use XFOIL [12] to calculate coefficients at a Reynolds number of 200,000, and then Viterna's method [13] to extrapolate to the range $-180°$ to $180°$.

3.1. External torque and gyroscopic precession
In this section we use rotor F_1 under the operating conditions, $U = 7m/s$, $\gamma = 0°$, $\theta = 45°$, and tip speed ratio, $\lambda = 7$, to look at the motion about the hinge. In Figures 3 and 4, the polars

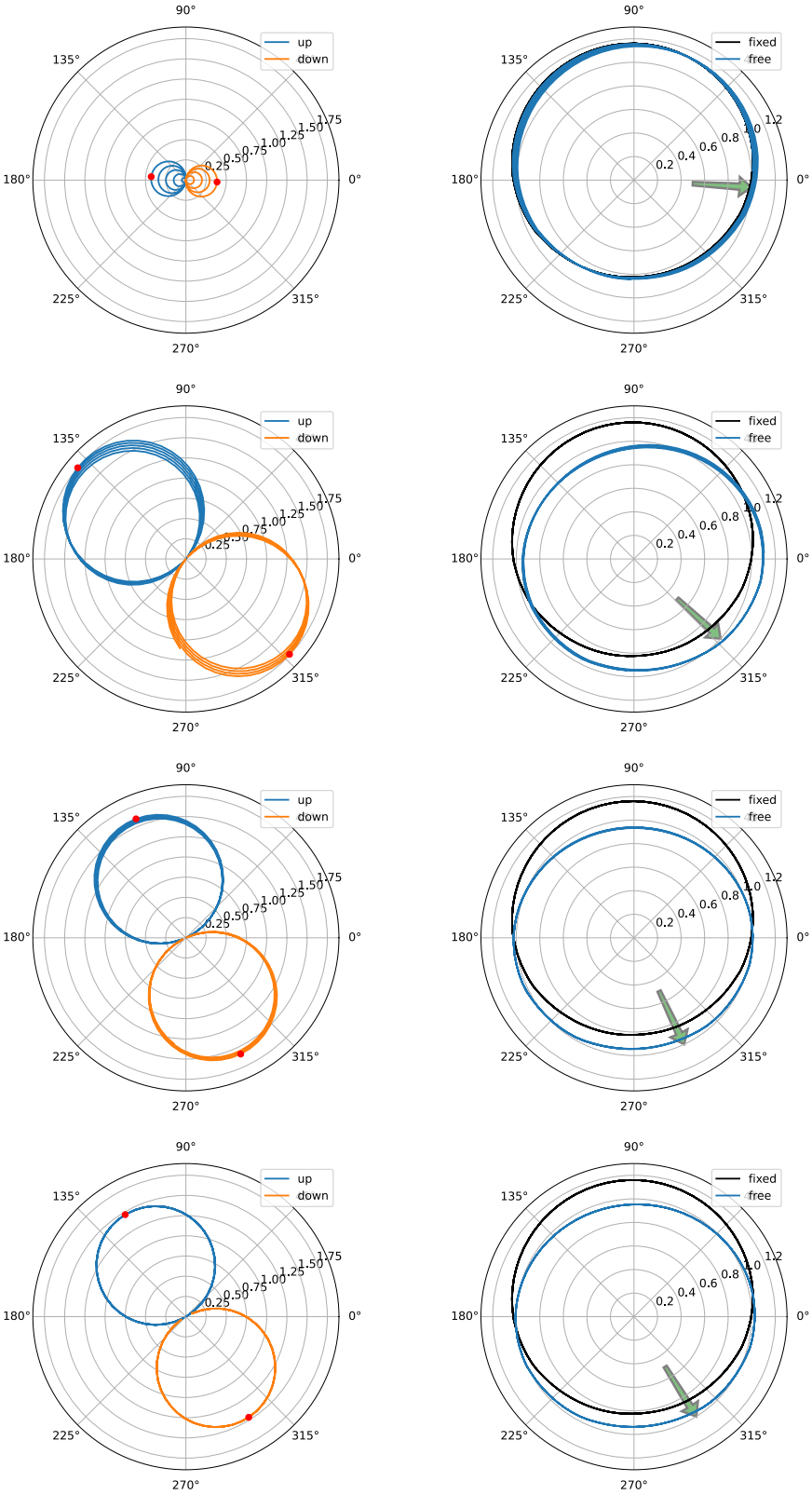

Figure 3: Gyroscopic precession of a two-bladed hinged rotor. Skewed wake model is turned off in the BEM solver. Plots top to down are instances from the time evolution of the hinge motion. On the left, growth of the rotor plane tilt is observed, and on the right, normalised lift integral polars depict the reduction in load variation.

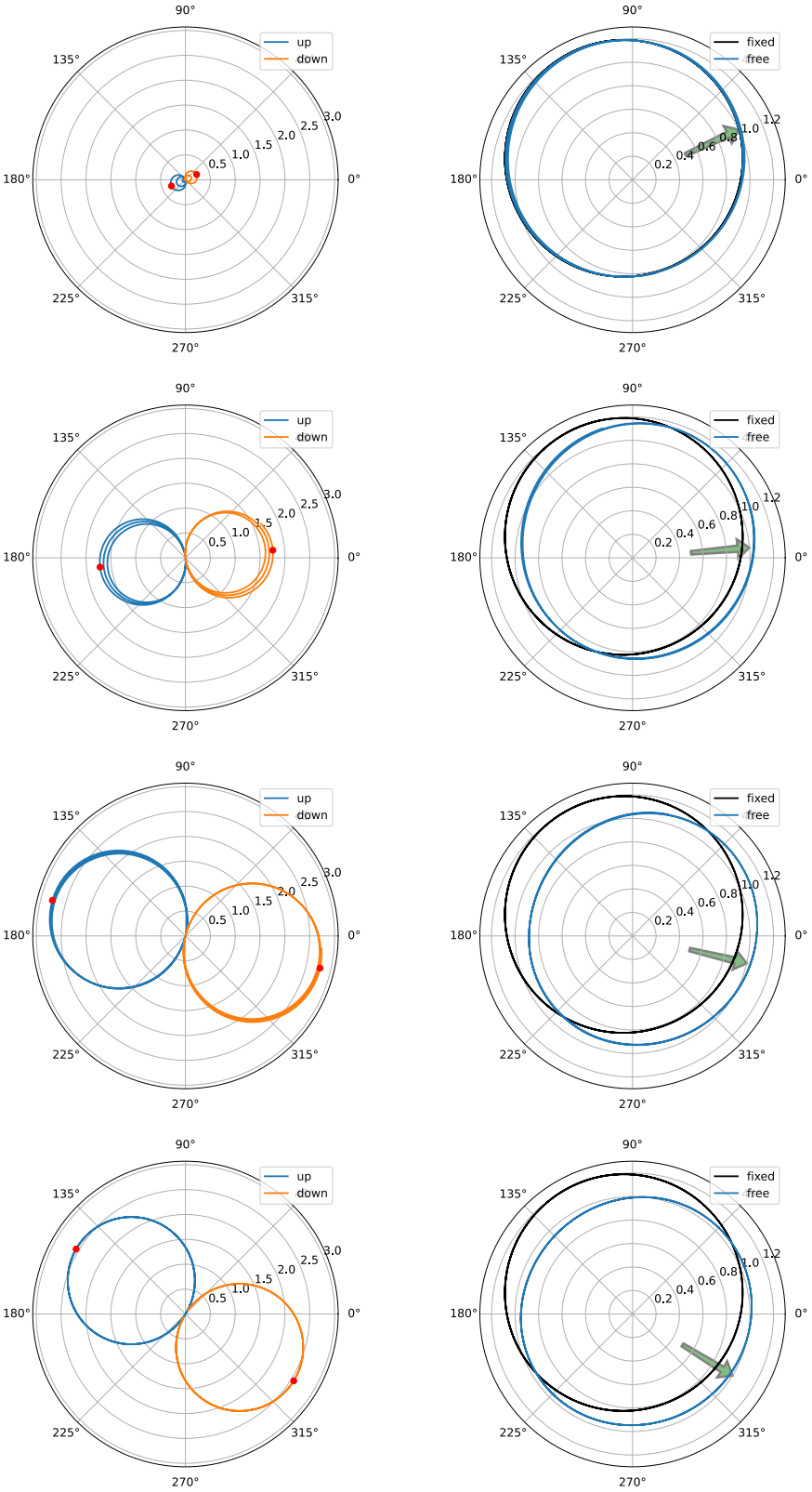

Figure 4: Gyroscopic precession of a two-bladed hinged rotor. Plots top to down are instances from the time evolution of the hinge motion. On the left, growth of the rotor plane tilt is observed, and on the right, normalised lift integral polars depict the reduction in load variation.

on the left hand side presents the time evolution of the absolute hinge rotation of a blade. The blue curve implies that the blade has tilted above the reference plane (positive hinge rotation), and the orange curve denotes the region where the blade has tilted below the reference plane. The red dots mark the maxima of the hinge rotations. From top to bottom, we see the absolute value of the hinge rotation growing, i.e, the tilt of the rotor plane. The polars on the right hand side are the normalised integral lift experienced by a blade: the blue curve for the load on the hinged rotor, and for reference, the black curve is the baseline unbalanced load experienced by an ordinary fixed rotor. Green arrows point towards the direction of the external torque.

For simplicity, in the first case (Figure 3), we turn off the skewed wake module and make dissymmetry of lift the only source of imbalance. The imbalance is purely geometric and therefore the direction of torque can be easily guessed. Due to gyroscopic precession, the rotor, and its momentum vector, start to tilt in the direction of torque, i.e., in the downwind direction. The feedback changes the external load and the direction of torque, and the rotor plane tilts further by following the torque in a positive feedback loop. The cycle continues until the imbalance in the aerodynamic load is negligible and the lift polar on the blade is a near perfect unit circle. The inertial forces on the blade prevent the rotor from reaching the ideal aerodynamic loading.

With the addition of the skewed wake model (Figure 4), we see a slightly larger imbalance in the aerodynamic loading. Furthermore, the initial direction of the torque, and therefore the direction in which the rotor plane starts tilting, are shifted into the approaching-downwind quadrant. Nevertheless, except for the phase shift in the direction of tilt, the gyroscopic precession of the rotor proceeds as before. The skewed wake effect which is orthogonal to the dissymmetry of lift simply rotates the net torque, and thereby the equilibrium position. In both cases, the rotor finds an equilibrium state of minimised variations in aerodynamic load, with the maximum of the hinge rotation in the approaching-upwind quadrant. However, with increased imbalance in the aerodynamic loading, the rotor plane sees a larger hinge rotation.

3.2. Limitations of the self correcting mechanism

Blade stall: The self correcting mechanism of the hinge depends on the negative correlation between lift and hinge rotation. On the low lift side, the rotor tilts down to increase the angle of attack so that lift would increase. And vice-versa on the high lift side so as to reduce lift. However, if the blade enters stall before reaching an equilibrium state, lift would sharply drop on the low lift side instead of increasing. Thus, the design loses its natural tendency to return to the reference position. To avoid this, the hinge needs to incorporate a range limiting mechanism. At high winds the need for such a mechanism may become acute.

Rotor sensitivity: While the hinge rotation is useful in relieving lift imbalance, the rotation has to be kept at a minimum to avoid unwanted inertial forces. Teeter, I_{yy}, is almost as dominant as the rotation of the blade, I_{xx}, which is the major component of inertia. Large hinge rotations are a result of either large imbalances in the lift dissymmetry, or slow aerodynamic response of the blade. Large imbalances in the lift dissymmetry can be a result of large misalignment angles or low tip speed ratios. Slow aerodynamic response can be a result of a low C_L over α performance of the aerofoil or a small hinge angle, δ_3. A small hinge angle converts most of the rotation into teetering and less into pitching. In all of these situations, large hinge rotations are required to make the necessary correction in lift.

Figure 5 demonstrates the same setup as before, but with the aerofoil F_2; which is only half as sensitive as F_1. Because of the weak aerodynamic response of F_2 compared to F_1, the growth in rotor tilt is slower compared to fig. 3. But, the final equilibrium rotor plane is almost twice as tilted as in fig. 3. Additionally, while the final lift polar of F_2 resembles that of F_1, we can clearly see the overshoots in the areas where the blade tried to correct itself. Teetering inertia

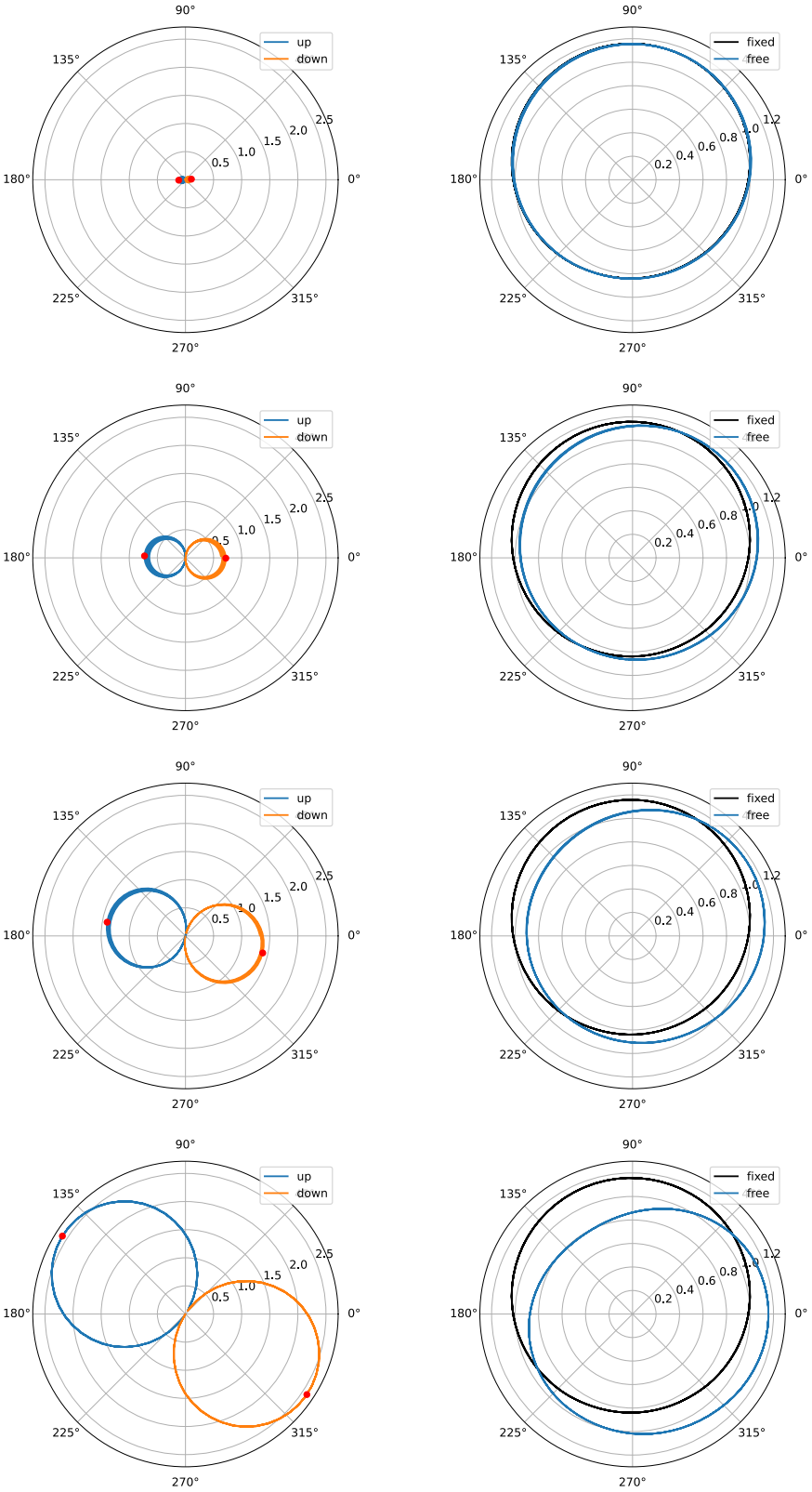

Figure 5: Precession and overshoot in the case of weak aerodynamic response. Plots top to down are instances from the time evolution of the hinge motion. On the left, growth of the rotor plane tilt is observed, and on the right, normalised lift integral polars depict uneven loads from the tilt overshoot.

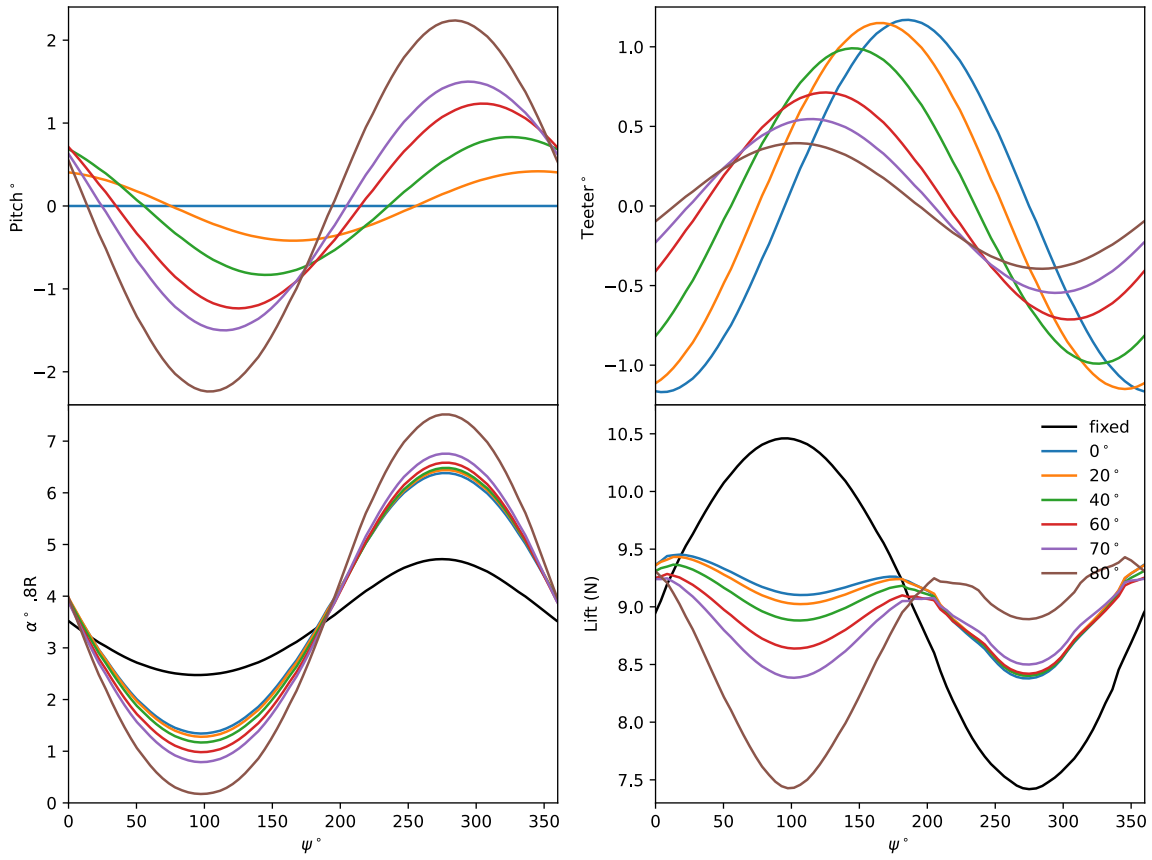

Figure 6: Performance of a rotor with varying δ_3 angles at steady state. Plots show the pitch (top left), teeter (top right), angle of attack at mid-span (bottom left), and integral lift (bottom right) on blade 1; blade 2 sees the same variations, but phased by an offset of 180°. Behaviour of a fixed-hinge rotor is also plotted for comparison.

(I_{yy}) from the larger hinge rotations and the weak aerodynamic response together causes the blade to overshoot and miss the ideal tilted plane.

Free rotation about the hinge is a passive mechanism. Also, we desire that the lift imbalance uses this degree of freedom to correct itself. However, as we noticed above, increased dissymmetry in the loads lead to larger hinge rotations, and thereby larger inertial forces. For the passive correction mechanism to work, aerodynamic forces have to be dominant and should be able to guide the blade as desired.

On the other hand, a fast responding rotor can cause overshoots from the pitching inertia (I_{zz}). Pitching response of the blade can be tweaked by selecting a high performance aerofoil or by increasing the δ_3 angle. The δ_3 angle is one of the most important parameters to look at in this design. Owing to the symmetry of a 2-bladed rotor, the design space to optimise δ_3 lies between 0° and 90°. By varying the δ_3, fig. 6 looks at the change in pitch, teeter, angle of attack at $0.8R$, and integral lift on one of the two blades. In this case we use F_3 (NACA4412). Additionally, the black curve marks the same for a fixed-hinge rotor.

In the case of the fixed-hinge rotor, the angle of attack varies between $\sim 2° - 6°$, and lift varies between $\sim 7.5 - 10.5$ N ($\sim \pm 16\%$ from the mean). For the free-hinge rotor with $\delta_3 = 0°$, the blades move in a pure teetering motion and therefore the pitch stays constant. Still, there is a sudden drop in the range in which lift varies to $\sim 8.5 - 9.5$ N ($\sim \pm 5\%$ from the mean). This

corresponds to the increased variation in the angle of attack induced by the teetering velocity ($\dot{\eta_z}$). Increasing the δ_3 angle, the blade starts to see pitching motion as well. This further reduces the gap in the lift variation, and slightly increases the oscillation in the angle of attack.

Pitch sensitivity increases with the δ_3. But, since the driving force of the motion is the lift force, a slight amount of teetering freedom is required to kickstart the hinge rotation. Therefore, barring the 90° case, $70° - 80°$ δ_3 blades are the most sensitive; they show significant pitching with less than 0.5° teetering. Low lift regions in the reference lift curve are brought up by pitching up. But, the slightest overshoot in the pitch down motion, to reduce the highs in the reference lift curve, causes the lift to drop a lot more than desired.

4. Conclusions

Introducing a hinge into the rotor for passive pitching of the blades expands the design space and it is necessary to incorporate hinge dynamics in the design toolchain. It is also important to investigate the sensitivity of the hinge mechanism to several parameters for the scalability of the concept. The key takeaways from this paper are, for a number of reasons, the extent of hinge rotation has to be limited. From an aerodynamics point of view, this will ensure that the blade does not hinge into its stall region. But for the design itself, this will avoid interference with the tower. Also, inertia of the blade will be a deciding factor in the scalability of this concept. With the blade tilting up and down about the hinge with a 1P frequency, there is a constant tug of war between aerodynamics and inertial forces. Lighter blades that can be easily steered are essential for scaling up.

Acknowledgments

The authors acknowledge support from the Rijksdienst voor Ondernemend Nederland (RVO) through the TSE Hernieuwbare Energie funding scheme for the project "TouchWind-PoP: Proof of principle for cost-effective floating offshore wind turbine concept" (TEHE119017). The authors would also like to thank Dr. Ricardo Pereira, Panos Georgopoulos, Eric Jansen, Pieter Riem, and other members of the TouchWind consortium for their fruitful discussions and feedback.

References

[1] Gaffey T M 1969 *Journal of the American Helicopter Society* **14** 49–67
[2] Perkins F W and Jones R 1981 The effect of δ_3 on a yawing hawt blade and on yaw dynamics *Wind Turbine Dynamics - NASA Conference Publication 2185*
[3] Henderson G M, Haines R S and Quarton D C 1989 The analysis and design implications of pitch-teeter coupling *Proceedings of the European Wind Energy Conference*
[4] Hohenemser K and Swift A 1984 *Journal of Solar Energy Engineering* **106** 171–176
[5] Swift A, Hohenemser K and Rangwala S 1985 The effect of hinge spring restraints on two-bladed, teetered wind turbine rotors *4th ASME Wind Energy Symposium*
[6] Hohenemser K 1987 Wind turbine yaw dynamics analysis for a teetered rotor system *6th ASME Wind Energy Symposium*
[7] Hohenemser K 1988 Wind turbine shut-down by self yawing *7th ASME Wind Energy Symposium*
[8] Hohenemser K 1995 Analysis and test results of a two-bladed, passive cycle pitch, hawt in free and controlled yaw Tech. Rep. TP-442-7391 NREL
[9] Malcolm D J 1999 *Wind Energy* **2** 79–98
[10] Ning S A 2014 *Wind Energy* **17** 1327–1345
[11] Kane T R and Levinson D A 1985 *Dynamics: Theory and Applications* (New York: McGraw-Hill Book Company)
[12] Drela M 1989 Xfoil: An analysis and design system for low reynolds number airfoils *Low Reynolds Number Aerodynamics* ed Mueller T J (Berlin, Heidelberg: Springer Berlin Heidelberg) pp 1–12
[13] Viterna L A and Janetzke D C 1982 Theoretical and experimental power from large horizontal-axis wind turbines Tech. Rep. TM-82944 NASA